# *Control of Flow Limitation in Flexible Tubes*



**Citation:** Wang, Ruo-Qian, Teresa Lin, Pulkit Shamshery, and Amos G. Winter. "Control of Flow Limitation in Flexible Tubes." Journal of Mechanical Design 139, no. 1 (October 3, 2016): 013401.

**As Published:** http://dx.doi.org/10.1115/1.4034672

**Publisher:** ASME International

**Persistent URL:** http://hdl.handle.net/1721.1/109244

**Version:** Final published version: final published article, as it appeared in a journal, conference proceedings, or other formally published context

**Ruo-Qian Wang**[1]
Mem. ASME
Department of Mechanical Engineering,
Massachusetts Institute of Technology,
Cambridge, MA 02139
e-mail: rqwang@mit.edu

**Teresa Lin**
Department of Mechanical Engineering,
Massachusetts Institute of Technology,
Cambridge, MA 02139

**Pulkit Shamshery**
Department of Mechanical Engineering,
Massachusetts Institute of Technology,
Cambridge, MA 02139

**Amos G. Winter V**
Mem. ASME
Assistant Professor
Department of Mechanical Engineering,
Massachusetts Institute of Technology,
Cambridge, MA 02139
e-mail: awinter@mit.edu

# Control of Flow Limitation in Flexible Tubes

*This paper proposes a new Starling resistor architecture to control flow limitation in flexible tubes by introducing a needle valve to restrict inlet flow. The new architecture is able to separately control the activation pressure and the flow rate: The tube geometry determines the activation pressure and the needle valve determines the flow rate. A series of experiments were performed to quantify the needle valve and the tube geometry's effect on flow limitation. The examined factors include the inner diameter, the length, and the wall thickness. A lumped-parameter model was developed to capture the magnitude and trend of the flow limitation, which was able to satisfactorily predict Starling resistor behavior observed in our experiments.* [DOI: 10.1115/1.4034672]

## 1 Introduction

This paper presents a parametric description of the behavior of Starling resistors in order to quantitatively predict their flow rate and activation pressure. A Starling resistor is a device consisting of an elastically collapsible tube mounted inside a static pressure chamber [1] (Fig. 1(*a*)). The key parameters that determine the operation of a Starling resistor are the upstream pressure ($P_1$), the downstream pressure ($P_2$), and the external pressure ($P_e$). The transmural pressure acting on the flexible tube ($P_e - P_2$) can be controlled such that it collapses the tube in proportion to increases in the upstream pressure to cause flow limitation. We are interested in describing the flow limitation case called pressure compensation, where after reaching an activation pressure, the flow rate remains constant with increases in the pressure driving the fluid flow (Fig. 1(*b*)). The activation pressure corresponds to the point of initial collapse of the flexible tube, which causes flow limitation. The ability to parametrically design Starling resistors to achieve a desired activation pressure and operating flow rate could be valuable to numerous industrial applications. For example, Zimoch et al. [2] demonstrated that pressure compensating Starling resistors could be designed to deliver the correct flow rate and activation pressure for low-cost drip irrigation.

We propose a novel Starling resistor architecture, where the pressure-driven flow and the transmural pressure are generated from the same source (Fig. 2). An inlet restrictor is used, in our case a needle valve, to reduce the pressure at the inlet of the flexible tube, increasing the transmural pressure acting over the tube. With this architecture, the flexible tube geometry and material dictate the activation pressure of the Starling resistor, and the inlet restrictor determines the flow rate during pressure compensating behavior. In this paper, we present a theoretical model which enables designers to choose inlet resistance and flexible tube design to achieve a desired flow rate and activation pressure.

Experimental studies on the flow inside flexible tubes are numerous, which are extensively reviewed by Bertram [3], Grotberg and Jensen [4], and Heil and Hazel [5]. Early flow limitation work was summarized and reproduced by Brower and Noordergraaf [6]. They confirmed that flow limitation behavior can be affected by tube geometry, and formed an empirically derived relationship to predict the flow rate versus inlet pressure behavior. Recent investigations have typically focused on one or more particular factors of flexible tube flow: The effect of the tube wall thickness was studied with thick-wall tubes [7,8], thin-wall tubes [9], and taper-wall tubes [10]; the effect of material was investigated using Penrose rubber [6] and Latex/Silastic rubber [7]; the effect of fluid viscosity was examined by Bertram and Tscherry [11]; and other investigated factors have included the periodic variation of the upstream and downstream flow rates [12,13] and testing square-shaped cross sections [14]. In conventional Starling resistors, the activation pressure and flow rate are determined by the nonlinear interplay of these factors, and there is no easy way to separately control them. To address this issue, the present study investigates the Starling resistor architecture in Fig. 2, which enables full control of flow rate via the needle valve, without changing activation pressure.

To deterministically design a Starling resistor with a given flow rate and activation pressure, a reliable theoretical model is required to connect the design of the inlet valve and flexible tube to their flow limiting performance. Shapiro [15] proposed that flow limitation occurs when the mean velocity of the flow matches the wave speed of the collapsible tube wall. His model was successful in reproducing the major characteristics of collapsible tube flow, such as choking and asymmetric deformation. Cancelli and Pedley [16] extended the model by introducing the axial tension of the tube, which allows the addition of the second boundary condition—the circular shape of the tube at the downstream rigid support. These models were unable to quantitatively predict the experimental or numerical simulation results until Whittaker et al. [17]. They derived an eigenvalue model that could quantitatively match the three-dimensional numerical simulation results of elliptical tube flows. Since the present study aims to create a parametric model that simplifies and guides the mechanical design of the Starling resistor with a circular cross section, we limit the scope of our study to a lumped-parameter model which provides experimentally validated prediction of flow limitation and avoids sophisticated numerical computations.

[1]Corresponding author.

Contributed by the Design Engineering Division of ASME for publication in the Journal of Mechanical Design. Manuscript received February 5, 2016; final manuscript received August 28, 2016; published online October 3, 2016. Assoc. Editor: Yu-Tai Lee.

  

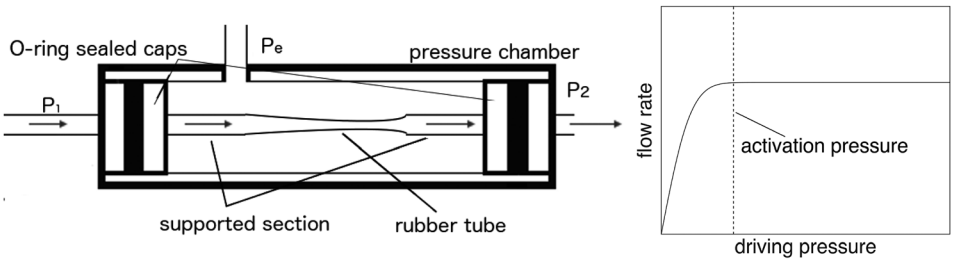


**Fig. 1 Starling resistor design and behavior: (*a*) a conventional Starling resistor design; (*b*) the concept of pressure compensation, where flow rate becomes constant if the driving pressure is beyond an "activation pressure" threshold**

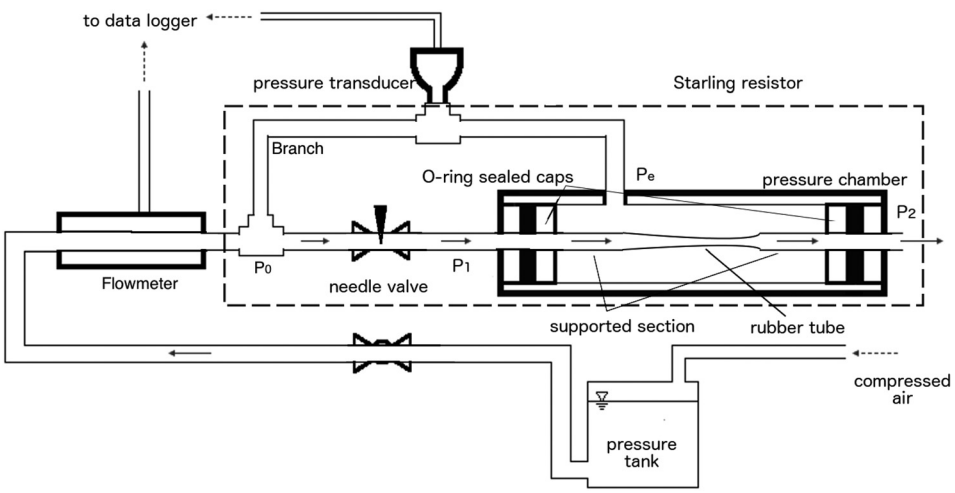


**Fig. 2 The experimental setup used in the present study: the modified Starling resistor architecture is enclosed in the dashed line and the pressure chamber is the same as that shown in Fig. 1(*a*)**

## 2 Experimental Method

Our experimental setup included a pressure supply, a measurement system, and a modified Starling resistor (Fig. 2). The system was driven by static pressure from a pressure tank, which was pressurized by compressed air and controlled by a pressure regulator. The pressure could range from 0 to 200 kPa (0–2 bar). The pressure tank was connected to the Starling resistor through a high-resolution rotor flow meter (Seametrics SES-050-13) with a measurement range of 6.3–630 mL/s (0.1–10 gal/min) and a resolution of 1605 pulse/gal. A branch was installed downstream of the flow meter to pressurize the pressure chamber, and a pressure transducer (Setra model 209 with a measurement range of 0–172 kPa and a dynamic response time of 5 ms) was installed at the branch to monitor the pressure. The pressure at the branch is denoted by $P_0$. Since the water could be treated as static in the branch and in the chamber, the measurement of the transducer was equal to the pressure at the T-junction point at the beginning of the branch, which was also equal to the pressure in the chamber. The pressure transducer and the flow meter were connected to a data logger to record the real-time signal with a sampling rate of 2000 Hz. Thus, the sampling frequency was much greater than the observed oscillation frequency of the tube (<120 Hz).

In the pressure chamber, two sets of O-ring sealed caps were manufactured with different barb-fittings to mount different diameter rubber tubes (McMaster-Carr 5234K97 and 5234K261). Two pressure chambers were used to vary the length of the tube (Fig. 1(*a*)). We introduced a needle valve (Swagelok Integral Bonnet Needle Valve, 1/4 in. diameter, requiring 9.5 turns to fully close) after the branch and before the pressure chamber. The needle valve and the control of $P_1$ and $P_e$ from a single source are the novel aspect of this experimental setup. Traditional Starling resistor setups have independent controls for the pressures $P_1$ and $P_e$ from different sources.

We performed a series of experiments on this test platform with various commercially available latex rubber tubes. We varied the following parameters: the inner diameter, the unsupported length, and the wall thickness of the tube. The average Young's modulus ($E$) of 1.96 MPa was given by the manufacturer for the extent of stretch used in our experiments. The experimental configurations are detailed in Table 1. Two experimental results extracted from Refs. [8] (case G) and [9] (case H) are also listed for comparison. To make sure no air bubbles were trapped in the chamber during assembly, we first fully filled the chamber and tilted and shook it to drive the bubbles out. Then, we started a small overflow through the connection point between the branch and the chamber in order to prevent air from entering. During the experiment, the chamber was fully closed at all times.

Each case in Table 1 was tested using different needle valve settings, ranging from fully opened to fully closed. Each test had three repeated trials, and the results presented in Sec. 3 are averaged if not claimed otherwise. In each trial, the pressure tank was slowly pressurized from 0 to 200 kPa and then decreased to zero, which are referred to as pressurizing and depressurizing scenarios, respectively. The variable

$$K_p = \frac{2}{3}\frac{E}{1-\nu^2}\frac{h^3}{D^3} \tag{1}$$

is a parameter proportional to the bending stiffness of the tube wall, where $E$ is the modulus of elasticity, $\nu$ is the Poisson's ratio,

**Table 1 Parameters of the experiment**

| Case | Inner diameter $D$ (cm) | Length $L$ (cm) | Wall thickness $h$ (mm) | Young's modulus $E$ (MPa) | $h/D$ | $K_p$ (kPa) | $c_0$ (m/s) |
|---|---|---|---|---|---|---|---|
| A | 0.635 | 23.5 | 0.794 | 1.96 | 0.125 | 3.40 | 1.84 |
| B | 0.635 | 31.5 | 0.794 | 1.96 | 0.125 | 3.40 | 1.84 |
| C | 1.27 | 23.5 | 1.59 | 1.96 | 0.125 | 3.40 | 1.84 |
| D | 1.27 | 31.5 | 1.59 | 1.96 | 0.125 | 3.40 | 1.84 |
| E | 0.635 | 23.5 | 1.59 | 1.96 | 0.25 | 27.2 | 5.22 |
| F | 0.635 | 23.5 | 2.38 | 1.96 | 0.375 | 91.9 | 9.59 |
| G | 1.3 | 22.1 | 2.39 | 3.40 | 0.184 | 18.7 | 4.32 |
| H | 1.2 | 122.1 | 1.00 | 3.15 | 0.083 | 1.63 | 1.28 |

and $h$ and $D$ are the wall thickness and diameter of the tube, respectively. The nominal wave speed of the tube structure is

$$c_0 = \sqrt{\frac{K_p}{\rho}} \tag{2}$$

where $\rho$ is the density of the water ($1000\,\text{kg/m}^3$ at room temperature).

## 3 Experimental Results and Discussion

Flow limitation experimental results are presented in terms of flow rate versus driving pressure. The pressure is the reading from the pressure transducer (Fig. 2) and represents the pressure difference from the pressure chamber to atmosphere. Inside the flexible tube, the pressure difference from the end of the unsupported section to the outlet is negligible compared to the pressure change along the unsupported section because of the small ratio of the supported section's length to its diameter. Thus, the pressure measurement from the transducer can be considered as the transmural pressure applied at the end of the unsupported tube.

Two distinctly different flow limitation modes were found (Fig. 3): mode 1, where the flexible tube begins to oscillate at $P \approx P_a$, and mode 2, where the tube steadily collapses after $P > P_a$, and then oscillates at a higher pressure. The results in the figure are original data for a single trial. Each result includes two curves: the solid curve was obtained in the pressurizing scenario, and the dashed line was from the depressurizing scenario. The pressure variation process is also shown by the arrows in the figure. The difference between them is due to the hysteresis stemming from the nonlinear tube deformation and the nonlinear flow dynamics.

In Fig. 3(*a*), the flow rate increased with the square root of the pressure at the beginning of the test, following the solid line while the tube had no significant deformation. After reaching the peak, a periodic oscillation suddenly occurred and the flow rate decreased to an approximately constant level. In the depressurizing scenario (dashed line), the flow rate was initially constant and then fell back to the zero point. Oscillation was present until the point that the peak flow rate occurred. Later, the magnitude and the frequency of the oscillation decayed. In comparison, the start of the oscillation was sudden, but the stop of the oscillation was a continuous and gradual process. The two curves by the two pressure variation scenarios almost overlapped except around the peak flow rate. The characteristics of the oscillation are shown in Fig. 4 for the case of Fig. 3(*a*). The peak-to-peak pressure amplitude was found highest at 89 Hz. This mode of the fluid–structure interaction was commonly observed in small diameter tubes, i.e., in cases A, B, E, and F. In the following discussion, we define activation pressure, $P_a$, as the pressure where the flow rate peaks and $Q_L$ as the approximately constant flow rate in flow limitation. Flow limitation is considered to happen at $P > P_a$ in this mode.

Mode 2 in Fig. 3(*b*) is more complex and was found in cases C and D. Similar to mode 1, the flow rate initially increased with the square root of the pressure until reaching $P_a$, with no deformation in the tube cross section. After the peak, the flow rate dropped gradually, while the tube was steadily squeezed and the cross-sectional area decreased until the flow dropped to the lower limit of the flow meter. In the depressurizing scenario, the flow rate increased abruptly and overshot the pressurizing scenario (i.e., the flow rate increased from zero and exceeded the flow rate obtained from the pressurizing scenario). The difference in flow rate depended on how quickly the pressure was decreased. The flow rate then fell back to the value of the pressurizing scenario when

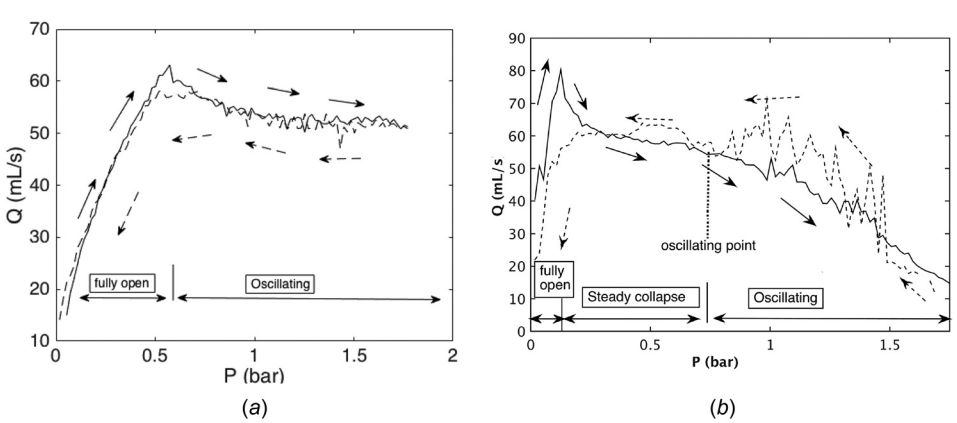


**Fig. 3 Characteristic experimental results from a single trial, without averaging: (*a*) mode 1 (case E with $k_{vn} = 21$): at low pressure, the flexible tube retains a circular shape (fully open). Oscillation occurs when $P \approx P_a$; (*b*) mode 2 (case C with $k_{vn} = 4$): the flexible tube retains a circular shape (fully open) at $P < P_a$, and then steadily collapses as $P > P_a$ until the oscillation starts at a higher pressure (solid line: the pressurizing scenario; dashed line: the depressurizing scenario; and arrows: the direction pressure was varied).**

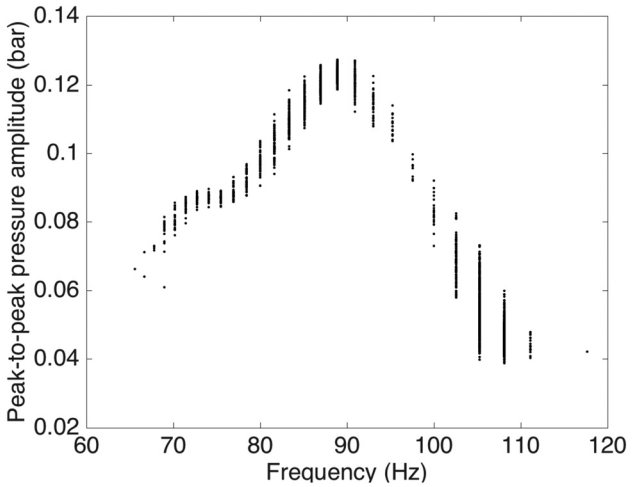


**Fig. 4 The peak-to-peak pressure amplitude at various oscillation frequencies for the case of Fig. 3(*a*)**

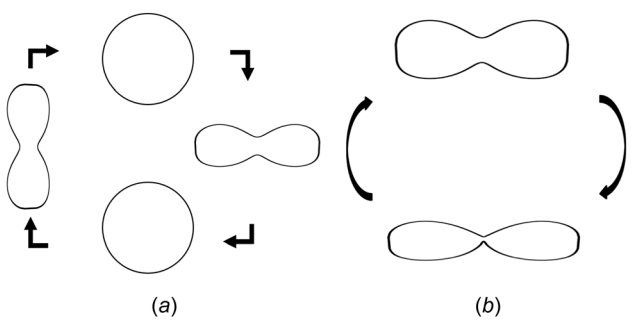


**Fig. 5 Sketch of the two types of oscillation discovered in Ref. [19]. (*a*) Type I: the wall oscillates between two nonaxisymmetric extremes. (*b*) Type II: the wall performs small-amplitude oscillations about one of the two nonaxisymmetric extremes.**

the oscillation decayed. It followed a lower route to reach the zero point due to hysteresis.

The different behaviors in the two modes confirmed the numerical simulation results of Heil and Waters [18]. As shown in Fig. 5, they reported two types of oscillations, including (I) the tube wall oscillation between two collapsed extremes (Fig. 5(*a*)) and (II) a small-amplitude oscillation about one of the extremes (Fig. 5(*b*)). Modes 1 and 2 in our study correspond to type (I) and (II) oscillations, respectively. In addition, Heil and Waters [18] claimed that the type of oscillation strongly depends on the cross-sectional area prior to the oscillation. Specifically, type (I) starts from the fully open and undeformed cross-sectional area, whereas type (II) starts from a reduced cross-sectional area. This report is consistent with our observation, i.e., mode 1 occurs when the tube is fully open and the mode 2 occurs after a steady collapse.

We observed that the flow limitation behavior was dependent on $dP/dt$. To ensure the repeatability of our experiments, we always used the minimum pressure variation rate ($\sim$0.03 bar/s) to simulate a quasi-steady state. The trials were conducted until three repeatable cases with the same trend and a similar order of magnitude were recorded, and the following results were obtained by averaging the flow rate at the same pressure from the three repeats. As each of the points in the experimental results was derived by averaging over $\sim$0.5 s, the error introduced by the averaging method is proportional to the inverse of the frequency of the tube oscillation. For the lowest oscillation frequency of 6.5 Hz in the present study, we reached the maximum error, which was estimated to be 11% after averaging the three trials of each case.

The present experiment employed a novel way to induce a transmural pressure by introducing a needle valve, rather than a separate external pressure. The resistance coefficient of the valve was determined by measuring its flow rate at different driving pressures (Fig. 6(*a*)), i.e., $k_v = P_v/[(1/2)\rho u_v^2]$, where $P_v$ is the pressure drop over the valve and $u_v$ is the mean velocity at the inlet of the valve. In the following, we use the nominal resistance coefficient, $k_{vn}$ (the $k_v$ value at 40 ml/s) to indicate the valve opening.

The effect of the needle valve can be observed by comparing tests with the same flexible tube geometry but different valve openings (Fig. 6(*b*)). The limited flow rate $Q_L$ was found to decrease with a small valve opening, while $P_a$ was roughly the same. This insight is a useful characteristic that can separate the control of $P_a$ from $Q_L$. The rubber tube geometry dictates $P_a$, and the flow rate can be changed using the needle valve without affecting $P_a$.

Another observation about Fig. 6(*b*) is that the flexible tube suddenly fully closed at the highest pressure, cutting off the flow. This stopping pressure decreased with smaller valve openings. In the depressurizing scenario, the flow rate had a spike from zero before a flow was initiated, at which point the flexible tube had a sudden opening. The pressure of the spike was also lower than the

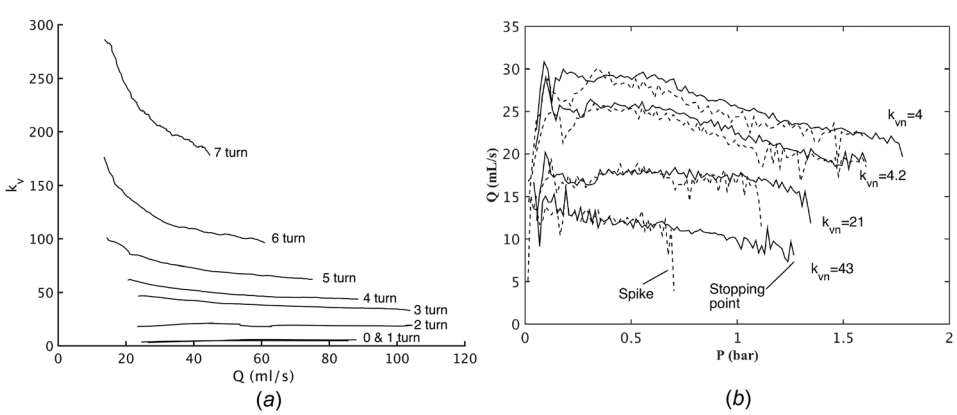


**Fig. 6 The effect of the needle valve on flow limitation: (*a*) the pressure drop coefficient $k_v$ with different valve openings and flow rates; (*b*) the effect of the needle valve openings for case B—a decreased opening corresponded to a low flow rate, but the activation pressure was roughly unchanged (the stopping point indicates a flow cutoff at the highest pressure in the pressurizing scenario and the spike indicates a sudden opening of the flexible tube in the depressurizing scenario)**

stopping point due to hysteresis or system bistability. Note that the present experiment was not designed to identify the experimental parameters that determine the cutoff point. In the same case, where the flow limitation behavior was repeatable and consistent, we observed significant variation in the cutoff and spike points. We suspect there are one or more parameters not characterized in our analysis that can determine the cutoff behavior. Determining the origins of this behavior is beyond the scope of the present study; we expect to do a systematic exploration in the future.

Comparing cases C and E, we can find the effect of the inner diameter of the flexible tube on flow limitation (Fig. 7(*a*)). The major difference introduced by the diameter is the different flow-limitation modes that have been discussed above. In terms of the characteristic parameters, the smaller inner diameter has higher $P_a$ and $Q_L$.

Three wall thicknesses (cases A, E, and F) were chosen to show the sensitivity of wall thickness on flow limitation (Fig. 7(*b*)). These experiments were performed with the same $k_{vn} = 21$. Initial flow rate increases with pressure were similar among these tests. With different wall thicknesses, the flow rate stopped rising at different peak pressures—the thicker wall sustained a higher $P_a$, which resulted in a higher $Q_L$. These results are consistent with our observation of the tube deformation: In the first rising section, the tube remains fully open and circular in shape; thus, the initial flow resistance was the same for all three cases due to their identical inner diameters. The thicker wall tube deformed at a higher pressure, because it had a greater bending stiffness and required a stronger transmural pressure to collapse.

The effect of flexible tube length on Starling resistors was studied previously, focusing on self-excited oscillation [20], but to the authors' knowledge, the present study is the first exploration of its effect on flow limitation. Figure 8 shows the length effect with different tube diameters. Comparing cases A and B with $k_{vn} = 4$ (Fig. 8(*a*)), the longer tube had a higher flow rate in the oscillation stage. In comparison with the large diameter tubes with $k_{vn} = 21$ (Fig. 8(*b*)), the shorter tube had a higher flow rate at $P_a$, but the longer tube had a higher mean flow rate after the self-excited oscillation started. In the depressurizing scenario, the longer tube followed a much higher flow rate until reaching the oscillation onset point, where the two pressure-decreasing curves converged.

## 4 A Simple Theoretical Model

To guide the design of Starling resistors with variable inlet restriction, a theoretical model was developed to predict the activation pressure $P_a$ and the limited flow rate $Q_L$. As reported by Grotberg and Jensen [4], no previous mathematical model can quantitatively predict the experimental results for Starling resistors. With a focus on the control of flow limitation, we make an effort to develop a lumped-parameter model to capture the trend and the magnitude of our experimental results. The present model is inspired by the seminal work of Shapiro [15]. Although this model is only valid for steady-state flow, it has a potential to

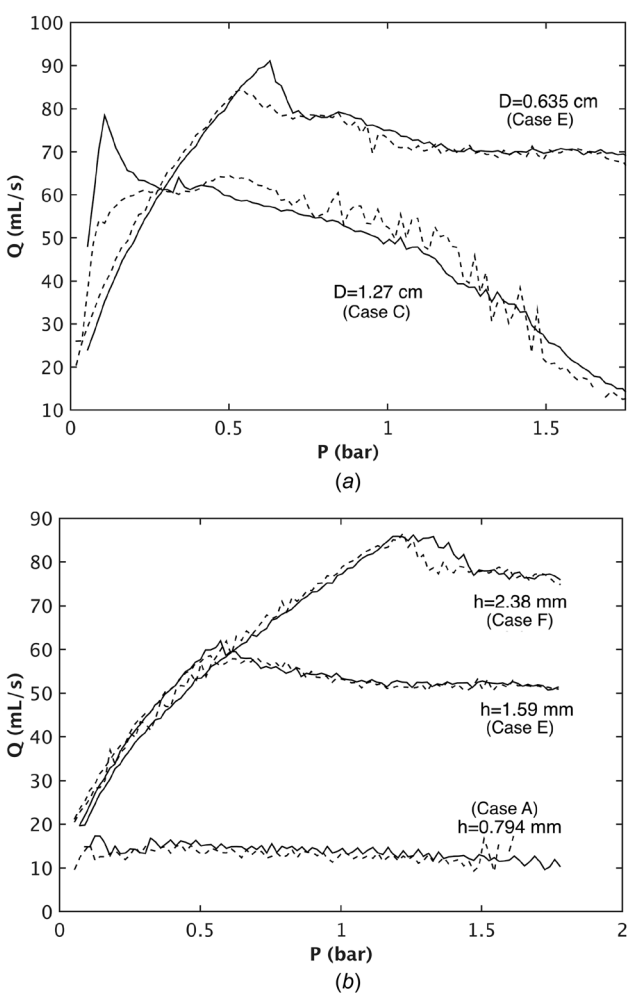


**Fig. 7 The effect of tube geometry on flow limitation: (*a*) the effect of the tube diameter with $k_{vn} = 4$; (*b*) the effect of the wall thickness with $k_{vn} = 21$**

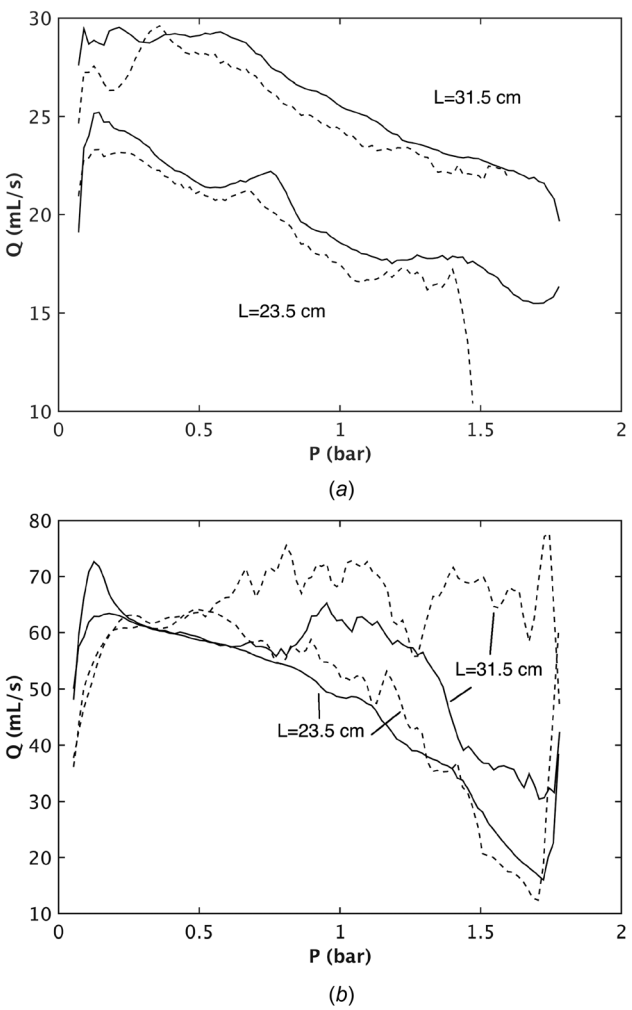


**Fig. 8 The effect of the tube length on flow limitation: (*a*) the comparison of cases A and B with $k_{vn} = 4$; (*b*) the comparison of cases C and D with $k_{vn} = 21$**

predict $Q_L$ and $P_a$, as they are determined by the onset of self-excited oscillation and the steady-state process before it. We found that a modification to Shapiro's model can predict our experimental results.

The deformation of the rubber tube is described by the "tube law," the relationship of the cross-sectional area and the transmural pressure. A theoretical 2D relationship derived by Flaherty et al. [21] and Shapiro [15] obtained a simple fitting formula after the opposite walls of the collapsed tube contact, i.e.,

$$\xi = (P_2 - P_e)/K_p = (A/A_0)^{-n} - 1 \tag{3}$$

$$\text{or} \quad A/A_0 = (\xi + 1)^{-\frac{1}{n}} \tag{4}$$

where $A$ is the average cross-sectional area, $A_0$ is the cross-sectional area before deformation, $n$ is the fitting exponent, and $\xi$ is the dimensionless transmural pressure. The most accurate fitting exponent reported, which captured pressure compensating flow limitation, was $n = 3/2$ [15].

The pressure loss from the T-junction to the end of the tube in Fig. 2 is caused by two factors: the resistance of the needle valve and the flexible tube. The pressure loss can be described by

$$P_2 - P_e \approx \frac{1}{2}\rho\left(k_v u_v^2 + k_t u^2\right) \tag{5}$$

where $u_v$ and $A_v$ are the flow velocity and the cross-sectional area inside the needle valve, $u$ is the average velocity in the flexible tube, $k_v$ is the pressure loss coefficient of the needle valve, and $k_t$ is the pressure loss coefficient of the flexible tube.

From mass conservation, we have

$$A_v u_v = Au \tag{6}$$

Substituting Eqs. (1), (2), and (6) into Eq. (5), we find that

$$\xi = \frac{P_2 - P_e}{K_p} \approx \frac{1}{2}\frac{u^2}{c_0^2}\left(k_v \frac{u_v^2}{u^2} + k_t\right) = \frac{1}{2}\frac{u^2}{c_0^2}\left(k_v \frac{A^2}{A_v^2} + k_t\right) \tag{7}$$

We can define the nondimensional flow rate as

$$q = \frac{Q}{A_0 c_0} = \frac{A}{A_0}\frac{u}{c_0} \tag{8}$$

Substituting Eq. (4) into Eq. (8) and eliminating $u/c_0$ using Eq. (7), we obtain

$$\begin{aligned} q &= (\xi + 1)^{-\frac{1}{n}}\left(\frac{2\xi}{k_v\left(\frac{A}{A_v}\right)^2 + k_t}\right)^{\frac{1}{2}} \\ &= \left(\frac{2\xi}{k_t(\xi+1)^{\frac{2}{n}} + k_v\left(\frac{A_0}{A_v}\right)^2}\right)^{\frac{1}{2}} \end{aligned} \tag{9}$$

Rewriting Eq. (9)

$$q \times \left(k_v\left(\frac{A}{A_v}\right)^2 + k_t\right) = (\xi + 1)^{-\frac{1}{n}}(2\xi) \tag{10}$$

which can be plotted (Fig. 9) with $n = 3/2$ to demonstrate that the flow rate reaches the maximum at a certain $\xi$.

To find out the maximum flow rate, we take the derivative of Eq. (9), and let $dq/d\xi = 0$, which leads to

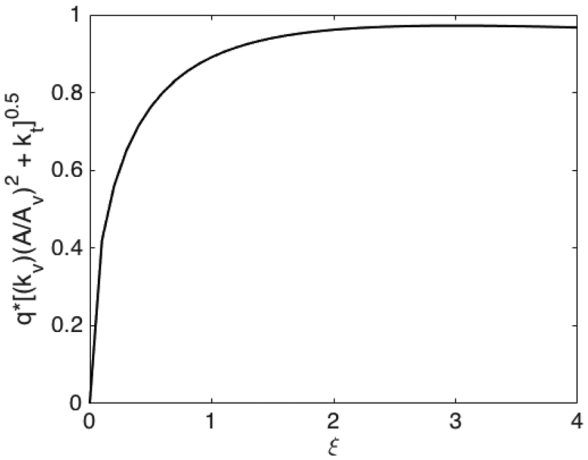


**Fig. 9 An example of the relationship expressed by Eq. (10) with $n = 3/2$**

$$\left(\left(\frac{2}{n} - 1\right)\xi - 1\right)(\xi + 1)^{\frac{2}{n}-1} = \frac{k_v}{k_t}\left(\frac{A_0}{A_v}\right)^2 \tag{11}$$

The solution to Eq. (11) is denoted by $\xi^*$, which is the nondimensional activation pressure. A comprehensive discussion on the determination of the activation pressure can be found in Ref. [15].

Given a particular design, the geometric parameters of $A_0$ and $A_v$ and the material parameter $n$ are fixed. The activation pressure $\xi^*$ is merely a function of $k_v/k_t$. The value of $k_v$ can be determined from the opening of the valve, while $k_t$ can be determined from an in-depth analysis of the fluid–structure interaction as demonstrated by Whittaker et al. [17], which would be arduous in engineering practice. We have identified a more straightforward solution based on the special feature of decoupling the activation pressure from the limited flow rate by placing a variable resistance valve (needle valve in Fig. 2) at the inlet of the Starling resistor. As shown in the experimental results of Fig. 6(*b*), the activation pressure was independent of the valve resistance $k_v$. Thus, the variation of $k_v$ should not change the result of $\xi^*$. To ensure this is the case, we can assume

$$\frac{k_v}{k_t^*} = C_k \tag{12}$$

where $C_k$ is a constant representing the ratio of the resistance coefficients at the activation pressure, and $k_t^*$ is the corresponding tube loss coefficient. This assumption makes $\xi^*$ not a function of $k_v$ in Eq. (9). This assumption dictates that the time-averaged tube resistance is proportional to the needle valve. Although we do not know the fluid–structure mechanics that govern this behavior, our experimental results indicate that the assumption expressed by Eq. (12) is accurate.

Taking $n = 3/2$, it was found that $C_k = 0.05$ by fitting Eq. (11) to our experimental data (Fig. 10(*a*)). In the figure, cases A–E are shown with error bars that indicate the upper and lower limits of the activation pressure with $k_v$ in each case. The prediction by the theoretical model is shown with the dashed line, which goes through the middle of all the results including the cases from literature (cases G and H). Note that an inlet restriction valve was not present in cases G and H, so we assumed $A_v = A_0$.

Substituting the solution for $\xi^*$ into Eq. (9), we obtain an expression for the nondimensional maximum flow rate

$$q^* = C_q \sqrt{\frac{2C_k\xi^*}{k_v\left[(\xi^* + 1)^{\frac{2}{n}} + C_k\left(\frac{A_0}{A_v}\right)^2\right]}} \tag{13}$$

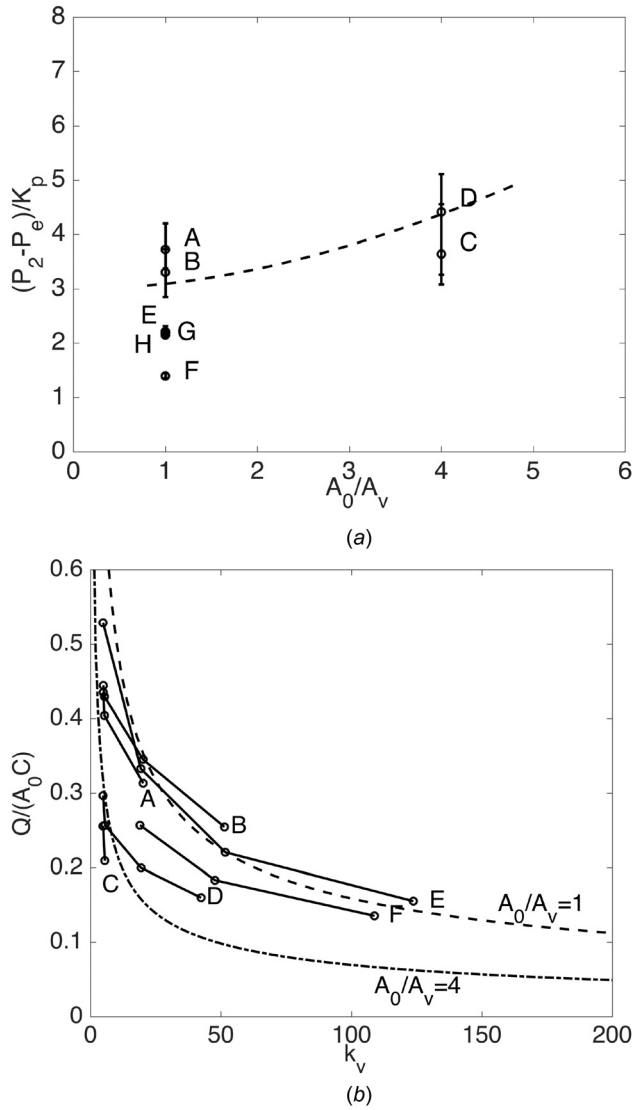


**Fig. 10 Comparison of experimental results with theory: (*a*) the comparison of activation pressure (dashed line: the prediction by Eq. (11)); (*b*) the comparison of limited flow rates (solid lines: experimental results; dashed line: the prediction by Eq. (13) with $A_0/A_v = 1$ to compare with cases A, B, E, and F; and dotted-dashed line: the prediction by Eq. (13) with $A_0/A_v = 4$ to compare with cases C and D)**

where $C_q = 9.5$ is a fitting coefficient to adjust the magnitude of the expression to our experimental results (Fig. 10(*b*)). The flow rate was found to decrease with higher $k_v$, as the valve resistance acts in series with the flexible tube resistance. The general trend is well predicted by Eq. (13). With the fitting coefficient $C_q$, Eqs. (11) and (13) could be used as parametric design tools to create Starling resistors based on the architecture in Fig. 2 with specified performance.

## 5 Considerations for Designing Products With Starling Resistors

The major feature of the present design is the decoupling of $P_a$ and $Q_L$, which enables a flexible design of self-regulating Starling resistors. With this knowledge, engineers could design resistors for different applications by first choosing the flexible tube geometry and material for a desired activation pressure, and then an inlet resistance (created by a needle valve, tortuous path, orifice, or other restrictor) to control flow rate. The branch connected from the upstream pressure source to the pressure chamber allows for a single pressure source both drive the fluid flow and induce a transmural pressure on the flexible tube.

A nontrivial issue in the practical use of a Starling resistor is the service life of the device, which may be largely determined by the collapsible tube. Hadzismajlovic and Bertram [22] performed fatigue testing on silicone-rubber tubes used in a pulsation generator (which behave similarly to those in our Starling resistor). They concluded that a tube could sustain 146–378 h of continuous work for a peak-to-peak downstream pressure amplitude of 220–310 kPa and frequency of 5.2–8.5 Hz. In comparison, the flexible tubes used in the present study had oscillation frequencies up to 120 Hz and a peak-to-peak pressure amplitude up to 70 kPa. An in-depth analysis of tube fatigue life is out of the scope of the present study, but the results presented in Ref. [22] indicate that Starling resistors could be used in applications that require days of continuous service, or much longer durations in intermittent service. Note that the life of flexible tubes will also be affected by a variety of environmental parameters including sunshine, moisture, and temperature. Any product created with the technology presented in this study should undergo field studies to fully understand its operational limitations.

## 6 Conclusion

In this work, a modified Starling resistor design is proposed that enables decoupled control of activation pressure and flow rate to achieve pressure compensating flow limitation.

A series of experiments were conducted to find a reliable means of controlling the activation pressure and the flow rate. Two flow limitation modes were found: In mode 1, the self-induced oscillation occurs at the peak of the flow rate, and in mode 2, it happens after a steady collapse of the flexible tube. Various key parameters were also examined, including the inner diameter, the length, and the wall thickness of the tube. Given the present examined parameter range, we found that (1) the inner diameter is the determining factor to the limitation mode: small diameter tubes demonstrated mode 1 and large diameter tubes demonstrated mode 2; (2) the tube length is able to increase the time-averaged flow rate in the oscillation regime of the flow limitation range, but not in steady state; and (3) the limited flow rate and activation pressure increase with tube wall thickness.

A lumped-parameter model was developed to capture the magnitude and trend of the flow limitation observed in experiments at various tube geometries. The trend and magnitude of the experiments were found to agree with our model.

## Acknowledgment

This research was sponsored by Jain Irrigation, Inc., and the Tata Center for Technology and Design at MIT. The authors thank Abhijit Joshi, Pawel Zimoch, Josh Wiens, and Natasha Wright for their input on this work.

## References

[1] Patterson, S. W., and Starling, E. H., 1914, "On the Mechanical Factors Which Determine the Output of the Ventricles," J. Physiol., **48**(5), pp. 357–379.
[2] Zimoch, P. J., Tixier, E., Joshi, A., Hosoi, A. E., and Winter, A. G., 2013, "Bio-Inspired, Low-Cost, Self-Regulating Valves for Drip Irrigation in Developing Countries," ASME Paper No. DETC2013-12495.
[3] Bertram, C. D., 2003, "Experimental Studies of Collapsible Tubes," *Flow Past Highly Compliant Boundaries and in Collapsible Tubes*, Springer, Dordrecht, Netherlands, pp. 51–65.
[4] Grotberg, J. B., and Jensen, O. E., 2004, "Biofluid Mechanics in Flexible Tubes," Annu. Rev. Fluid Mech., **36**(1), pp. 121–147.
[5] Heil, M., and Hazel, A. L., 2011, "Fluid–Structure Interaction in Internal Physiological Flows," Annu. Rev. Fluid Mech., **43**(1), pp. 141–162.
[6] Brower, R. W., and Noordergraaf, A., 1973, "Pressure-Flow Characteristics of Collapsible Tubes: A Reconciliation of Seemingly Contradictory Results," Ann. Biomed. Eng., **1**(3), pp. 333–355.
[7] Gavriely, N., Shee, T. R., Cugell, D. W., and Grotberg, J. B., 1989, "Flutter in Flow-Limited Collapsible Tubes: A Mechanism for Generation of Wheezes," J. Appl. Physiol., **66**(5), pp. 2251–2261.

[8] Bertram, C. D., and Castles, R. J., 1999, "Flow Limitation in Uniform Thick-Walled Collapsible Tubes," J. Fluids Struct., **13**(3), pp. 399–418.
[9] Bertram, C. D., and Elliott, N. S. J., 2003, "Flow-Rate Limitation in a Uniform Thin-Walled Collapsible Tube, With Comparison to a Uniform Thick-Walled Tube and a Tube of Tapering Thickness," J. Fluids Struct., **17**(4), pp. 541–559.
[10] Bertram, C. D., and Chen, W., 2000, "Aqueous Flow Limitation in a Tapered-Stiffness Collapsible Tube," J. Fluids Struct., **14**(8), pp. 1195–1214.
[11] Bertram, C. D., and Tscherry, J., 2006, "The Onset of Flow-Rate Limitation and Flow-Induced Oscillations in Collapsible Tubes," J. Fluids Struct., **22**(8), pp. 1029–1045.
[12] Low, H., and Chew, Y., 1991, "Pressure/Flow Relationships in Collapsible Tubes: Effects of Upstream Pressure Fluctuations," Med. Biol. Eng. Comput., **29**(2), pp. 217–221.
[13] Low, T. H., Chew, Y. T., Winoto, S. H., and Chin, R., 1995, "Pressure/Flow Behaviour in Collapsible Tube Subjected to Forced Downstream Pressure Fluctuations," Med. Biol. Eng. Comput., **33**(4), pp. 545–550.
[14] Walsh, C., Sullivan, P. A., Hansen, J., and Chen, L.-W., 2007, "Measurement of Wall Deformation and Flow Limitation in a Mechanical Trachea," ASME J. Biomech. Eng., **117**(1), pp. 146–152.
[15] Shapiro, A. H., 1977, "Steady Flow in Collapsible Tubes," ASME J. Biomech. Eng., **99**(3), pp. 126–147.
[16] Cancelli, C., and Pedley, J., 1985, "A Separated-Flow Model for Collapsible-Tube Oscillations," J. Fluid Mech., **157**, pp. 375–404.
[17] Whittaker, R. J., Heil, M., Jensen, O. E., and Waters, S. L., 2010, "Predicting the Onset of High-Frequency Self-Excited Oscillations in Elastic-Walled Tubes," Proc. R. Soc. A, **466**(2124), pp. 3635–3657.
[18] Heil, M., and Waters, S. L., 2006, "Transverse Flows in Rapidly Oscillating Elastic Cylindrical Shells," J. Fluid Mech., **547**, pp. 185–214.
[19] Weaver, D. S., and Paidoussis, M. P., 1977, "On Collapse and Flutter Phenomena in Thin Tubes Conveying Fluid," J. Sound Vib., **50**(1), pp. 117–132.
[20] Bertram, C. D., Raymond, C. J., and Pedley, T. J., 1990, "Mapping of Instabilities for Flow Through Collapsed Tubes of Differing Length," J. Fluids Struct., **4**(2), pp. 125–153.
[21] Flaherty, J. E., Keller, J. B., and Rubinow, S. I., 1972, "Post Buckling Behavior of Elastic Tubes and Rings With Opposite Sides in Contact," SIAM J. Appl. Math., **23**(4), pp. 446–455.
[22] Hadzismajlovic, D. E., and Bertram, C. D., 1996, "Collapsible-Tube Pulsation Generator for Crossflow Microfiltration: Fatigue Testing of Silicone-Rubber Tubes," J. Appl. Polym. Sci., **61**(4), pp. 703–713.